

Article

Spinning Disk Reactor Technique for the Synthesis of Nanometric Sulfur TiO₂ Core–Shell Powder for Lithium Batteries

Alessandro Dell’Era ^{1,*}, Francesca A. Scaramuzzo ¹, Marco Stoller ², Carla Lupi ²,
Marco Rossi ¹, Daniele Passeri ¹ and Mauro Pasquali ¹

¹ Department of Basic and Applied Sciences for Engineering, Sapienza University of Rome, via A. Scarpa 14, I-00161 Roma, Italy; francesca.scaramuzzo@uniroma1.it (F.A.S.); marco.rossi@uniroma1.it (M.R.); daniele.passeri@uniroma1.it (D.P.); mauro.pasquali@uniroma1.it (M.P.)

² Department Chemical Engineering Materials Environment, Sapienza University of Rome, Via Eudossiana 18, I-00184 Roma, Italy; marco.stoller@uniroma1.it (M.S.); carla.lupi@uniroma1.it (C.L.)

* Correspondence: alessandro.dellera@uniroma1.it

Received: 1 April 2019; Accepted: 3 May 2019; Published: 9 May 2019



Abstract: Sulfur/lithium battery performances are strictly related to the morphology and nanostructure of sulfur particles. In this work, a comparison of the morphological characteristics and electrochemical properties of electrodes based on colloidal sulfur (CS) obtained by means of traditional chemical precipitation from aqueous solution and via spinning disk reactor (SDR) has been performed. In particular, through the SDR technique and by using different fluid dynamic conditions, it was possible to obtain monodisperse and nanometric sulfur particles with higher electrochemical performances when used as the cathodic active material in lithium batteries. Moreover, a method to produce core–shell nanoparticles with sulfur and titanium dioxide, starting from a colloidal sulfur (S8) solution and produced by SDR, has been performed, obtaining good electrochemical results. In particular, the nanometric sulfur powder produced by the SDR technique showed a capacity higher than CS after 100 cycles, even if the capacity decreased rapidly in both cases. Instead, considering the core–shell S–TiO₂ material, the nanostructured electrode allowed a wide use of active material and a reduced capacity decay during cycling. Specifically, the material showed an initial capacity of 1395 mAh/g, i.e., representing 83% of the theoretical value, which decreased during operation up to 450 mAh/g after about 30 cycles. Then, the material capacity remained unchanged and no substantial loss of capacity was recorded up to 100th cycle.

Keywords: Lithium-sulfur battery; spinning disk reactor technique; S–TiO₂ core–shell structure; sulfur nanoparticles; cathode materials

1. Introduction

Over the years several methods for the production of sulfur nanoparticles (SNp) have been developed [1–4]; among these, the method of the microemulsion is one of the most important due to its flexibility and the excellent control over the size of the particles [5]. These methods use the same chemical reaction between sodium thiosulfate Na₂S₂O₃ and hydrochloric acid HCl, but in different fluid dynamic conditions.

In general, the preparation of colloidal sulfur (CS) has many advantages [1–6] such as:

- The synthesis takes place at room temperature in a single step.
- The process is scalable and uses cheap, non-toxic and easily available materials.

- The particles obtained are compatible with the traditional techniques to produce lithium batteries and enables the use of electrolytes, binder and conductive materials used in industry today.

The concentration of the reactants seems to be one of the most important aspects to control the final size of the particles [5,7–9]. In particular, the concentrated solutions of $\text{Na}_2\text{S}_2\text{O}_3$, under normal stirring conditions, cause excessive growth of the particles. On the other hand, excessively dilute solutions do not allow acceptable yields to be obtained and make the successive separation step of the material difficult. Then, the limits of such a procedure are represented by a poor yield (mass of sulfur in volume of solution) and the difficulty of producing nanometer-size particles. In order to obtain particles under submicron size, particularly dilute solutions have to be used to avoid agglomeration. Chaudhuri et al. [5,9] have shown that it is possible to get SNp with an average diameter of about 200 nm by using 5 mm aqueous solution of $\text{Na}_2\text{S}_2\text{O}_3$ and a stoichiometric amount of HCl. However, using different fluid dynamic conditions it is possible to synthesize monodisperse SNp through the spinning disk reactor (SDR) (or rotating disk reactor) technique. The SDR [10,11] consists of a rotary disc placed horizontally and confined in a cylindrical housing. The reagents, introduced at or near the center of the disc are quickly pushed outward by centrifugal force. In this way, a thin liquid film is formed on the surface of the disk, exhibiting high micro-mixing conditions at reduced residence time. In these conditions, the reaction takes place at the nanoscale and the final solution is collected at the basin of the reactor.

Then, the use of the SDR presents a series of advantages which can be summarized as follows:

- The conditions of micro-mixing can be obtained within the liquid film over the disc surface by using a low amount of energy.
- The reduced residence time and the high local supersaturation values limits the growth after the nucleation allowing the production of nanometric size particles.
- The use of concentrated solutions allows high yields to be obtained. In addition to this, the synthesis via SDR is a continuous production process that can be easily scaled up for industrial applications.
- The particle size distribution of the product may be controlled by means of the operating parameters such as flow rate of the reactants, rotating velocity of the disc and position of the reactant injectors over the disc surface [10,11].

Therefore, in particular, in this work we want to emphasize that by using the SDR technique under different fluid dynamics conditions, it is possible to obtain monodisperse and nanometric size sulfur particles having higher electrochemical performance as active material in lithium-ion batteries with respect to sulfur particles obtained by colloidal solution.

Another fundamental aspect to take into account is the capacity loss for Li-S cell due to the diffusion of polysulfides in solution. The lithium polysulfides (LiS_x $x = 4; 6; 8$) are extremely soluble in traditional electrolytes and their formation, during cycling, causes strong morphological and compositional changes inside the cathode. To overcome this problem, in literature there are two different strategies: (i) Prepare composite materials where sulfur is encapsulated in a carbonaceous [12–15] and polymer [16] matrix or a conductive network of graphite [14], carbon nanotubes [17,18] or graphene [19,20], (ii) synthesize core-shell particles in which sulfur is the core while the shell is often a conductive material or a metal oxide [15,21–25]. For the proper functioning of an electrochemical cell, the coating must ensure good electrical conductivity and good ionic and electronic contact. In this work the authors, already involved and interested in electrochemical study of electrode material for batteries [26–36], set up a method to produce core-shell nanoparticles with sulfur and titanium dioxide, starting from a CS (S8) solution produced by SDR and hydrolysis of titanium tetraisopropoxide $\text{C}_{12}\text{H}_{28}\text{O}_4\text{Ti}$ (TTIP) in a colloidal solution. Finally, a comparison with the electrochemical performances of material synthesized by using a more traditional way for CS preparation has been realized. By using the SDR technique it has been possible to obtain monodisperse sulfur nanopowders with an average diameter of about 60 nm, increasing the yield at the same time. The comparison of the materials obtained highlights that, keeping all the other conditions constant, the different fluid dynamic regimes

of the two techniques lead to the synthesis of particles with different size. In particular, SDR allows smaller particles to be obtained, which show higher electrochemical performances. Finally, the S–TiO₂ core-shell structure brings a reduction of capacity decay during cycling.

2. Experimental

2.1. Instruments

Scanning Electron Microscope (SEM) analyses were obtained by the high-resolution Auriga-Zeiss (Jena, Germany) Field Emission (FE)-SEM microscope. The apparatus is also equipped with an energy dispersive X-ray (EDX) detector (Bruker, Billerica, MA, USA). The size distribution was measured by dynamic light scattering (DLS Malvern, Worcestershire, UK, series PCS4700). The diffraction patterns were obtained by means of diffractometer Rigaku (Wilmington, MA, USA) using X monochromatic radiation (Cu-K α). The centrifugation was produced by using the ALC 4222 MKII centrifuge (Milan, Italy). The galvanostat used was Maccor (Tulsa, USA) Series 4000 placed inside a dry room at controlled relative humidity (RH) <20 ppm and an average temperature of 21 °C). Data were collected and analyzed through a special interface program (by LabView, 2009). The SDR consisted of a rotating disc with a diameter of 85 mm, equipped with two injectors placed in correspondence of its center and 10 mm above the surface. The apparatus also included two peristaltic pumps with variable flow.

2.2. Method

A comparison between two synthesis routes was performed. Sulfur nanoparticles were obtained either by (i) traditional chemical precipitation (CS) or by (ii) using the SDR technique followed by (iii) a coating with TiO₂, which led to a S–TiO₂ core-shell structure. The overall process is summarized in Figure 1. Finally, both cathodic materials were tested (iv) in an electrochemical cell, as successively detailed in Section 3.3.

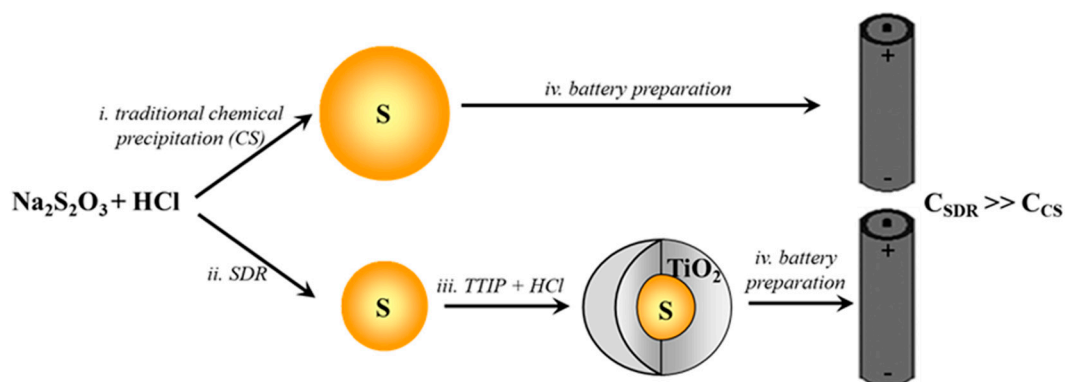


Figure 1. Overview of the process. Reactants and conditions: (i) Na₂S₂O₃ + HCl 1:2, 30 min, room temperature; centrifugation. (ii) Na₂S₂O₃ + HCl 1:2 at 1200 rpm disk rate; centrifugation. (iii) S by spinning disk reactor (SDR)+tetraisopropoxide (TTIP) + HCl, 2h, r.t.; centrifugation. (iv) cathode: Active material + C + Teflon 40:50:10; anode: Li; electrolyte: 1 M lithium bis(trifluoro methane sulfonyl imide (LTFSI) in dimethoxy ethane diethylene glycol dimethyl ether (DME:DEGDME) 1:1.

2.2.1. Sulfur Synthesis by Means of Traditional Chemical Precipitation from Aqueous Solution (CS)

The CS preparation was obtained by the reaction between Na₂S₂O₃ (Aldrich code:563188-100G) and HCl (Carlo Erba code:528525) in aqueous solution. The reaction can be written as follows:



The colloidal solution was centrifuged at 4000 rpm for 30 min in order to separate the particles. Finally, to remove the waste products such as NaCl the powder was rinsed in distilled water and

centrifuged again. The product was dried under vacuum at room temperature overnight before being used in an electrochemical cell.

2.2.2. Synthesis by Means of SDR

For the SNp synthesis by means SDR, 200 mL aqueous solution of $\text{Na}_2\text{S}_2\text{O}_3$ at 4.3 M concentration was prepared. Separately, a stoichiometric quantity (1:2 by mol) of HCl was diluted in 200 mL of distilled water. The pump was set to 100 mL/min while the test was conducted at 1200 rpm disk rate. Once the depletion of the reactants was reached, the solution was collected for subsequent centrifugation. Finally, as before, to remove NaCl the powder was rinsed in distilled water and centrifuged again. The product was dried under vacuum at room temperature overnight before being used in an electrochemical cell.

2.3. Core–Shell Synthesis (S–TiO₂)

The proposed method consists in a TiO₂ coating of sulfur particles present in a colloidal suspension produced by a SDR reactor. Fifty milliliters of the colloidal solution were collected and poured into a beaker. Separately, 1 mL of concentrated TTIP (Aldrich code: 377996-100ML) was diluted in 20 mL of isopropyl alcohol. The solution was added dropwise to the colloidal suspension previously obtained together with 10 mL of HCl under magnetic stirring. The reaction was allowed to proceed for 2h. The final suspension was finally centrifuged at 4000 rpm for 30 min. Subsequently, the material was rinsed in distilled water and centrifuged again at 4000 rpm for 15 min. The product was dried under vacuum at room temperature overnight. By weighing the material before and after the coating it was possible to estimate that the wt.% of sulfur within the obtained cathode material was about 48%.

3. Results and Discussion

3.1. DLS Analysis

In order to estimate the size of the particles obtained, they were analyzed by DLS. One milliliter of an aqueous solution of particles with a concentration of 1 mg/mL was used, obtaining a concentration independent measure. In Figure 2 the analysis results are reported. For CS material (Figure 2a), the largest number of particles had an average diameter in the range from 580 nm to 600 nm, while for SDR (Figure 2b) most particles had a diameter in a range from 50 to 70 nm, which means ten times smaller than those produced by simple colloidal solution reaction.

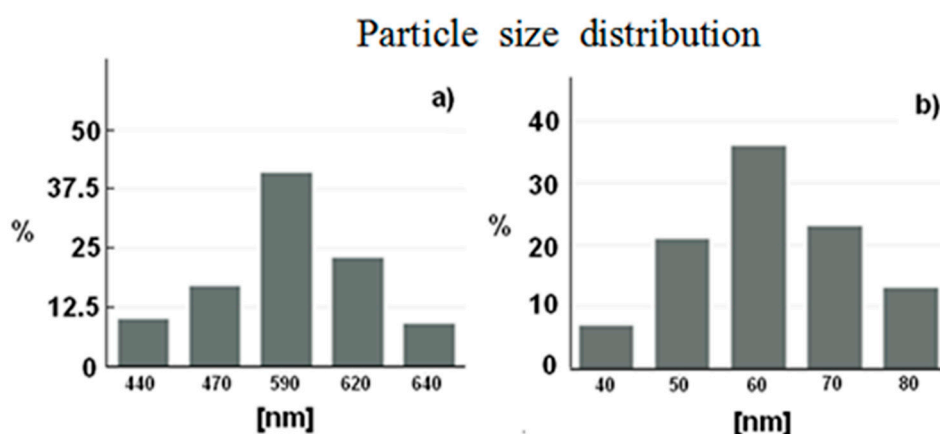


Figure 2. (a) Particle size distribution of sulfur particles produced by precipitation from colloidal solution; (b) particle size distribution of sulfur particles produced by SDR.

3.2. SEM and XRD Characterization

For sample preparation, a drop of highly diluted CS solution synthesized according to Reaction (1) was deposited on an appropriate stub and dried at room temperature overnight. Morphological characterization was performed by SEM analysis. In Figure 3a it is possible to notice the dispersion and size distribution of particles obtained by CS. The image shows an average diameter of about 1 μm .

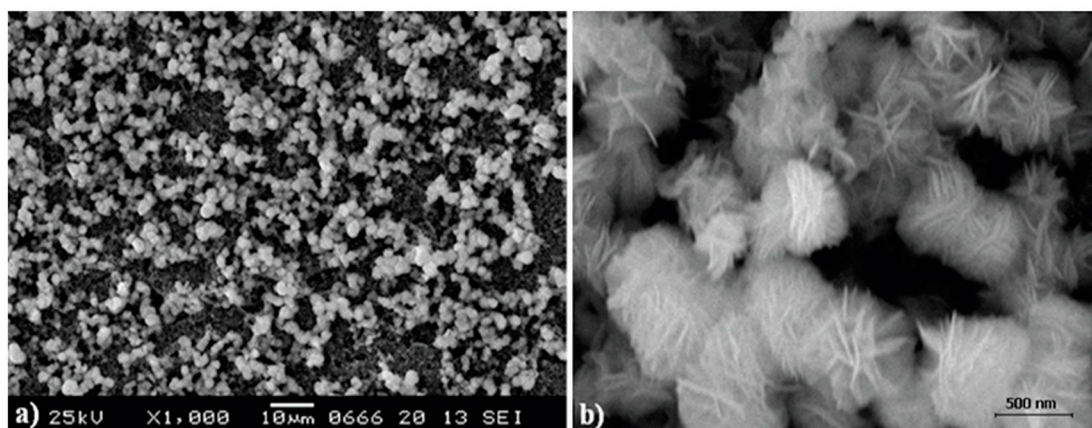


Figure 3. (a) SEM image of the sulfur particles produced by means colloidal sulfur (CS) solution; (b) particles at 10,000 \times magnification.

The observed values were higher than those found by DLS, because DLS measurements were carried out in solution, thus preventing the particle agglomeration undergone in the drying process. Figure 3b shows a detail of the particles in an image with 10,000 \times magnification. Besides the spherical shape, a characteristic lamellar structure is visible. In Figure 4, a SEM image of the sulfur particles produced by means of SDR is reported. The particles have a spherical shape and the size distribution is in agreement with the results obtained through DLS analysis. In particular, on the picture the diameter of a particle is reported equal to 82 nm. In Figure 5, two micrographs of the S-TiO₂ particles at different magnifications are presented. The core-shell particles have a spherical shape and are sufficiently dispersed.

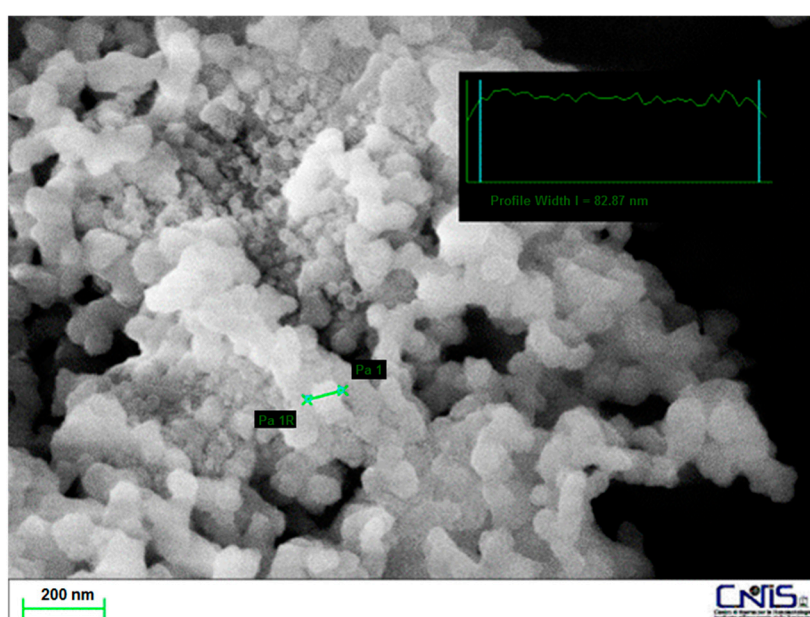


Figure 4. SEM image of the sulfur particles produced by means of SDR.

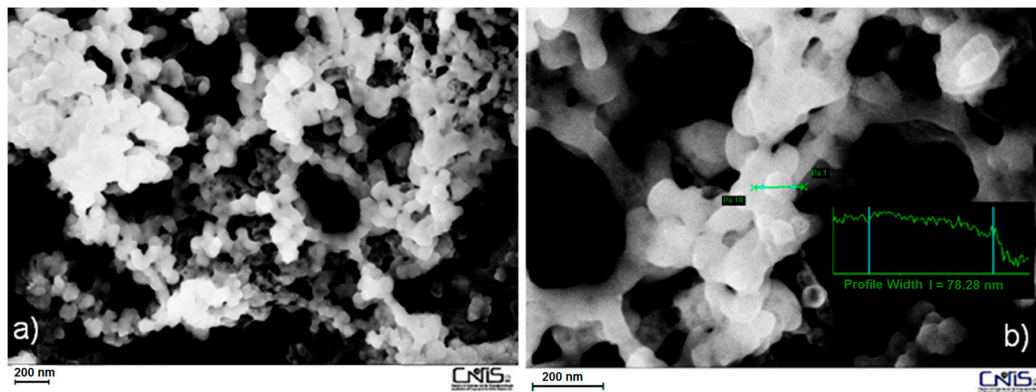


Figure 5. (a) A SEM image of S-TiO₂ core-shell particles;(b) a detail of the same image reporting the size of a particle.

The average size can be estimated by referring to the micrograph in Figure 5b. The image shows an average size of particles produced between 75 and 100 nm. Compared to the method of Cui et al. [21] the process used produced particles, on average, 10 times smaller. In Figure 6 the selected area for the EDX study and the corresponding energy spectra are presented.

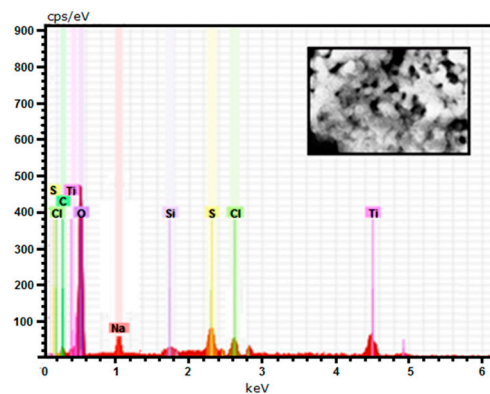


Figure 6. Energy dispersive X-ray (EDX) spectra of S-TiO₂ structures related to the onset selected area (800 nm × 500 nm).

Both peaks related to sulfur and titanium can be observed, thus confirming the coverage of the particles by TiO₂. However, a little bit of NaCl was also detected. The presence of Si peak is due to the silicon support on which the material has been placed for SEM-EDX analysis. The sulfur and titanium distribution is represented by EDX maps in Figure 7a,b respectively. Since the dots referring to titanium are sparser than those related to sulfur, it is possible to argue that, despite the core-shell configuration expected, a more homogeneous TiO₂ coating is desirable.

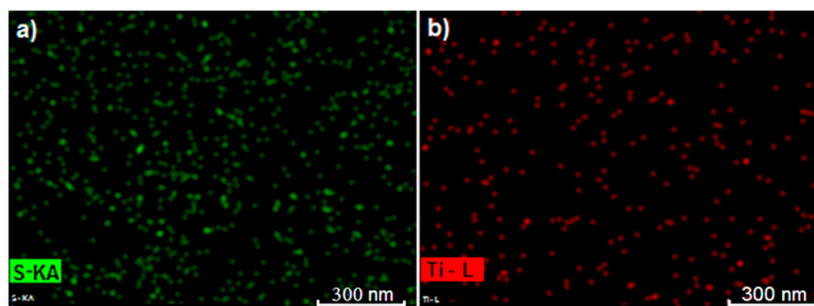


Figure 7. EDX maps for S (a) and Ti(b) for a sample of S-TiO₂.

Figure 8 shows the diffractometric patterns of the S-TiO₂ samples. The Crystallographic Open Database (C.O.D.), an open-access collection of crystal structures of organic, inorganic, metal-organics compounds and minerals, has been used to identify the orthorhombic sulfur phase (C.O.D. codes: 1537087). Moreover, since the spectrum of S-TiO₂ nanopowders presents peaks of low intensity, it is possible to deduce that the material is not highly crystalline, especially when compared with the results obtained by other authors [1,37,38]. Actually, the peaks of TiO₂ are absent, thus highlighting that the coating is amorphous. Some impurities like NaCl are also present in both cases (C.O.D. codes: 9006376).

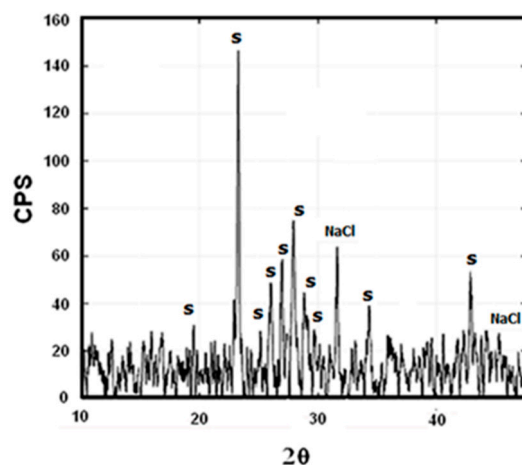


Figure 8. Diffractometric pattern of S-TiO₂ particles.

3.3. Electrochemical Characterization

The materials prepared through the colloidal solution, by either CS or SDR technique, have been used for cathode preparation. The electrode was prepared by mixing together in a mortar the active material, powder of super S carbon and Teflon in the form of ribbon in 40:50:10 weight ratio. Successively the resulting mixture was laminated obtaining a tape from which 1 cm² round electrodes were punched. In a typical preparation, the electrode weight was about 7.5 mg, which means a sulfur loading of about 3 mg/cm² for CS and SDR materials and of 1.4 mg/cm² for core-shell S-TiO₂ material. For electrochemical characterizations, a T shape cell with lithium metal as anode, LTFSI lithium bis(trifluoro methane sulfonyl imide) 1 M in DME:DEGDME (dimethoxy ethane diethylene glycol dimethyl ether) 1:1 by volume and as the electrolyte and the material to be tested as cathode, was assembled. Two wool glass separators soaked with the electrolyte solution were used. All tests were performed in a voltage range from 1.6 to 2.8 V and using a constant specific current of 167.5 mA/g (C/10, where C is the theoretical capacity). Figure 9a shows the discharge curves relative to the first, third, fifth and tenth cycle for a material obtained through CS.

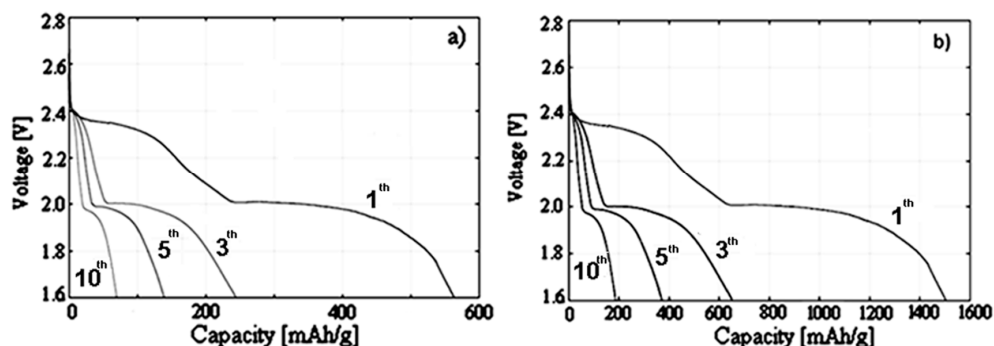


Figure 9. (a) Discharge curves at theoretical capacity (C)/10 for CS material; (b) discharge curves at C/10 for SDR material.

It is possible to recognize the typical trend of a Li–S cell with the presence of two distinct plateaus at different potential. The material had an initial capacity of 570 mAh/g, namely about 34% of the sulfur theoretical capacity. This value gradually decreased, reaching 70 mAh/g at the end of the tenth cycle, which means that the electrode lost 82% of its capacity during the first 10 cycles. Figure 10a shows the charging curves for the previously mentioned cycle. It can be noted that the capacity value relative to the first cycle was equal to 540 mAh/g, so it was lower than the value obtained during the discharge. This indicates that, once formed, Li_2S is not fully oxidized and does not completely participate in the subsequent electrochemical reactions. Furthermore, it is possible that the polysulphides in solution were reduced chemically to the anode to form a passivating layer on the metallic lithium. In Figures 9b and 10b, respectively, the curves of discharge and charge-sweeps relative to the first, third, fifth and tenth cycle for a material obtained through SDR are represented. The electrode showed a specific capacity for the first cycle of 1510 mAh/g, which represents 90.1% of theoretical capacity. This value dropped to 623 mAh/g during the third cycle to be around 197 mAh/g at the end of the tenth cycle. The high value of capacity during the first cycle demonstrates the effectiveness of using nanostructured materials for Li–S cell. In order to perform a fair comparison, the electrochemical materials were tested for 100 cycles under the same conditions. The results obtained are presented in Figure 11a,b, respectively, from which it clearly shows that the loss of capacity continues even after the tenth cycle for both materials: In detail, the cell passes from 70 mAh/g to 22 mAh/g losing 1.23% of initial value per cycle for the material obtained by CS, and from 197 mAh/g to 70 mAh/g with an average rate of loss equal to 1.53% per cycle for the material obtained by SDR. After the 20th cycle, the capacities were maintained substantially unchanged. In both cases the loss of capacity in the third discharge sweep was 55% with respect to the first one.

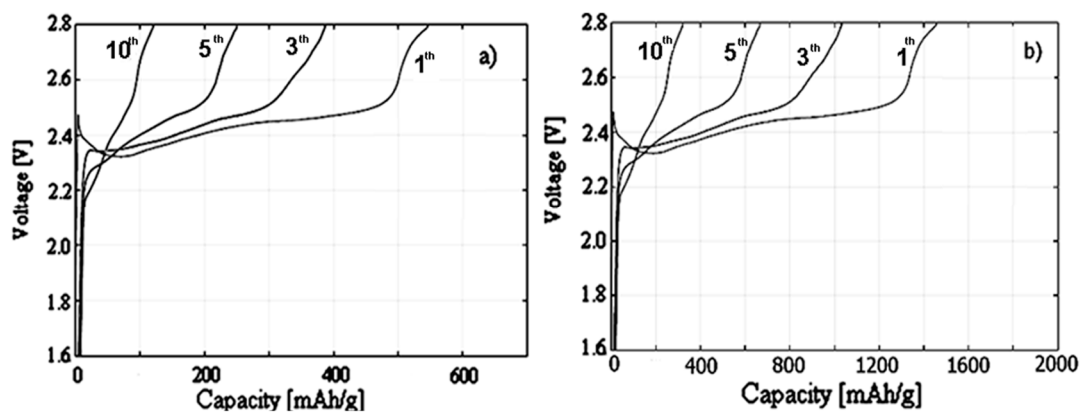


Figure 10. (a) Charge curves at C/10 for CS material; (b) charge curves at C/10 for SDR material.

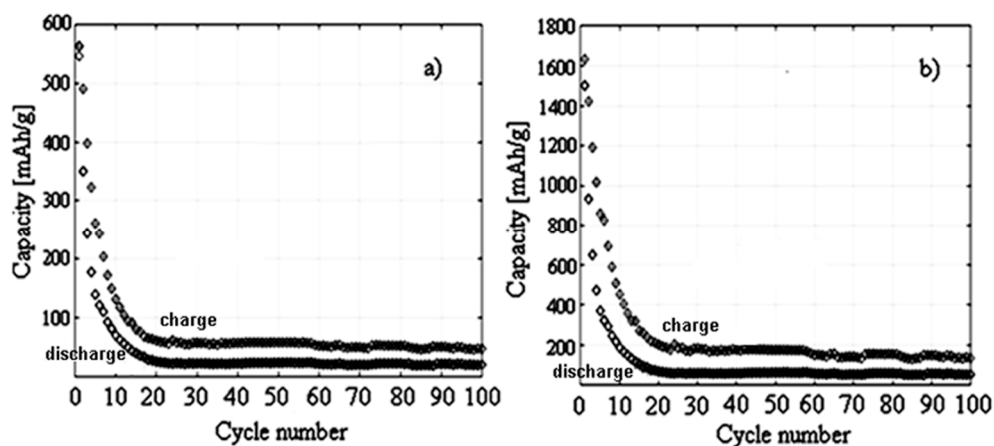


Figure 11. Trend as a function of cycle number (a) CS, (b) SDR.

The decrease of the particle size led to an increase of the initial capacity equal to more than twice: The greater the specific surface, the higher the amount of material involved in the lithium sulfides formation process. However, since smaller particle size means higher exposed surface, the dissolution of the high order sulfides [39] in the electrolyte during the cycling was observed as well. The problem may then be solved by producing a core-shell type structure. In fact, in this case it is possible to see as the percentage decrease of the capacity of the third discharge sweep, respect to the first one, was only about 7.7%, although also in this case the capacity tended to decrease for the first 20 cycles and then it stabilized to a value higher than in the two previous cases. Since EDX analysis suggested that the coating was not homogeneous, it is possible that part of the active material in the poorly covered zones still slowly dissolved, while where the core-shell was well formed there was a good retention of capacity. Moreover, most likely, after the first few cycles, the continuous variations of cathode volume caused the destruction of initial morphology of material. In particular, the strong expansion of elemental sulfur during the discharge process also involves the breaking of titanium dioxide rigid shell which surrounds the particles. However, since it forms a mechanical limit to polysulfide mobility, TiO_2 can absorb these ions preventing their spread within the electrolyte [40]. In Figure 12a,b, the curves for the first, third, fifth and tenth charge and discharge sweep, respectively, are shown for core-shell S- TiO_2 materials. With particular reference to the first discharge cycles, the capacity was 1395 mAh/g, namely about 83% of the sulfur theoretical value. The cell showed a value of 1290 mAh/g and 1270 mAh/g respectively during the third and fifth cycles, and around 1120 mAh/g at the end of tenth cycle. The loss of capacity was 18% of the initial value.

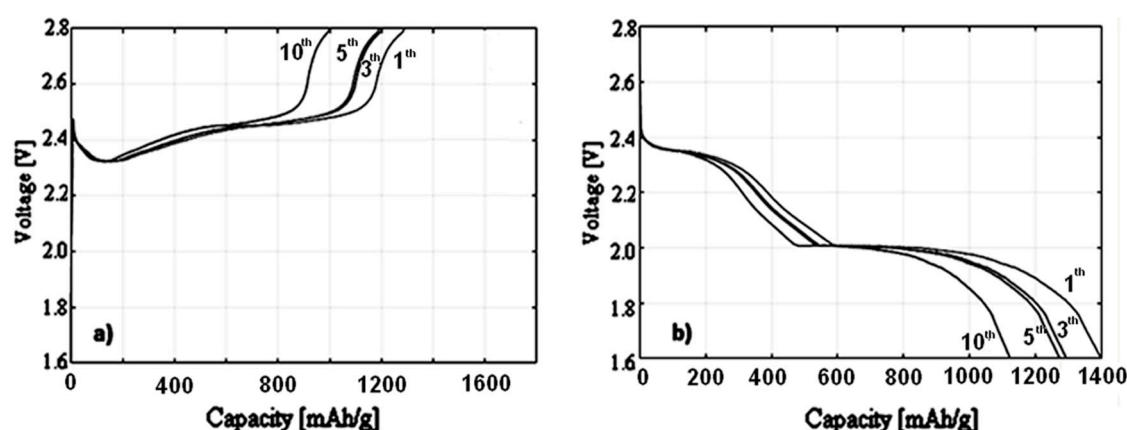


Figure 12. (a) Charge curves obtained at C/10 for first, third, fifth and tenth cycle and (b) discharge curves obtained for first, third, fifth and tenth cycle for core-shell S- TiO_2 materials.

In Figure 13 discharge and charge curves related to the thirteenth, seventeenth, fiftieth and hundredth cycle, are shown. It is possible to notice that the capacity measured after 50 cycles was 460 mAh/g, a value that remains, as said before, unchanged during subsequent cycles. The trend of capacity as a function of cycle number is presented in Figure 14. The cell, after the twentieth cycle, lost 63% of the initial value, even if it maintained a capacity of about 450 mAh/g at the end of the 100 cycles. The results obtained demonstrate the effectiveness of core-shell configuration in multi-functional design of a sulfur-based cathode. In particular, the high capacity observed during the first few cycles are attributable to the small size of particles which allows an almost total use of active material. Moreover, the presence of TiO_2 shell represents a barrier against polysulfides diffusion [21]. Although the material is still unable to deliver a capacity near the theoretical one, the results obtained in term of capacity are bigger with respect to the traditional cathodic material used nowadays in lithium-ion batteries.

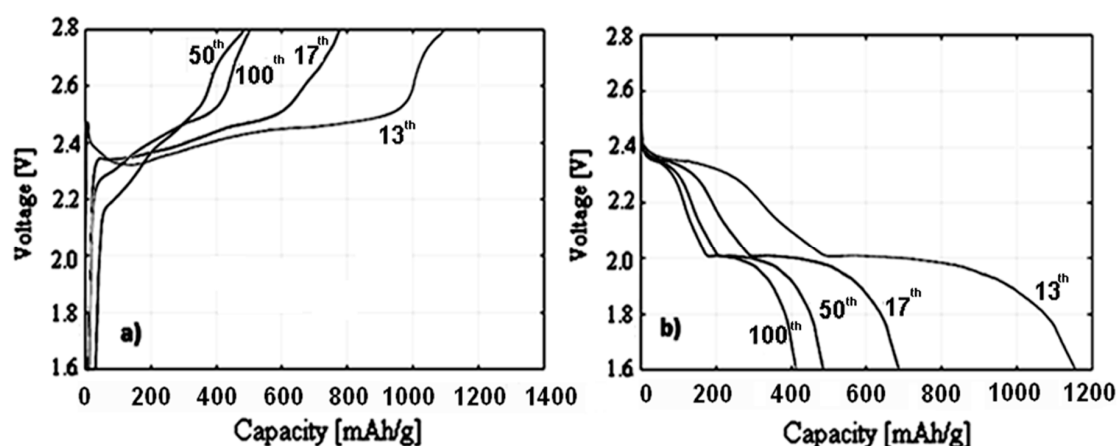


Figure 13. (a) Discharge curves obtained at C/10 for 13th, 17th, 50th and 100th cycle and (b) charge curves obtained for 13th, 17th, 50th and 100th cycle for core-shell S-TiO₂ materials.

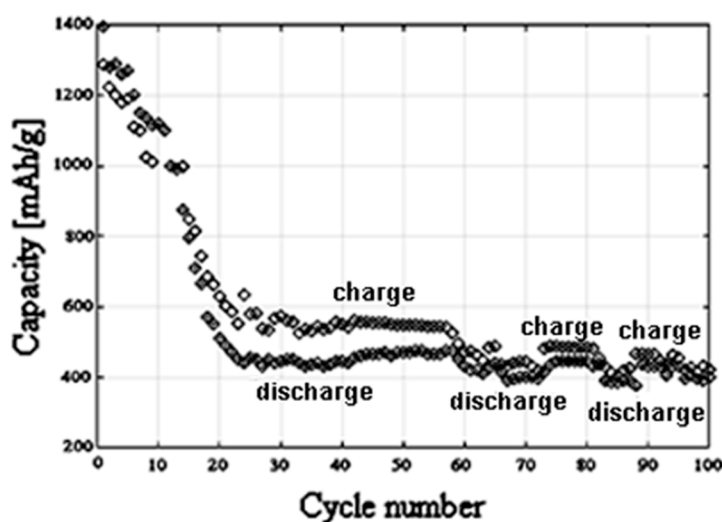


Figure 14. Capacity trend as a function of cycle number for core-shell S-TiO₂ materials.

4. Conclusions

In this work the electrochemical performances of cathodic electrodes based on monodisperse and nanometric sulfur particles have been analyzed. Generally speaking, regular shape and size allow a wider utilization of the active material which is related to a higher specific capacity. The use of the SDR technique allowed us to obtain monodisperse sulfur nanopowders with an average diameter of about 60 nm and to increase the process yield. The comparison between the two different materials investigated highlights that under equal conditions, but using different fluiddynamic regimes, it is possible to control the sulfur particle size. In particular, the nanometric sulfur powder produced by the SDR technique shows better characteristics and a capacity, after 100 cycles, more than three times superior to the one obtained using material produced by CS. As far as the core-shell S-TiO₂ material is concerned, the nanostructured electrode has allowed a wideuse of active material and a reduced capacity decay during cycling. In particular, the material showed an initial capacity of 1395 mAh/g equal to 83% of the theoretical value. The capacity of the electrochemical cell decreases during operation up to 450 mAh/g after about 30 cycles. Then, the material capacity remains unchanged and no substantial loss of capacity has been recorded up to 100th cycle. The results reported prove the effectiveness of core-shell structure for a new multifunctional active material design for Li-S cells. Despite the persistent problem of loss capacity, by means of S-TiO₂ core-shell particles, substantial improvements were obtained, which indicates the effectiveness of the proposed strategy. Greater

control of TiO₂ shell formation and the appropriate engineering of particles with blanks inside, can lead to even better results.

Author Contributions: M.S. and M.P. conceived and designed the experiments; A.D., M.P. and M.S. performed the experiments; A.D., F.A.S., C.L., M.R., D.P. analyzed the data; A.D. and F.A.S. wrote the paper.

Funding: This research received no external funding.

Conflicts of Interest: The authors declare no conflict of interest.

References

1. Deshpande, A.S.; Khomane, R.B.; Vaidya, B.K.; Joshi, R.M.; Harle, A.S.; Kulkarni, B.D. Sulfur Nanoparticles Synthesis and Characterization from H₂S Gas, Using Novel Biodegradable Iron Chelates in W/O Microemulsion. *Nanoscale Res. Lett.* **2008**, *3*, 221–229. [[CrossRef](#)]
2. Guo, Y.; Zhao, J.; Yang, S.; Yu, K.; Wang, Z.; Zhang, H. Preparation and characterization of monoclinic sulfur nanoparticles by water-in-oil microemulsions technique. *Powder Technol.* **2006**, *162*, 83–86. [[CrossRef](#)]
3. Guo, Y.; Deng, Y.; Zhao, J.; Wang, Z.; Zhang, H. Synthesis and Characterization of Sulfur Nanoparticles by Liquid Phase Precipitation Method. *Acta Chim. Sin.* **2005**, *63*, 337–340.
4. Xie, X.Y.; Zheng, W.J.; Bai, Y.; Liu, J. Cystine modified nano-sulfur and its spectral properties. *Mater. Lett.* **2009**, *63*, 1374–1376. [[CrossRef](#)]
5. Chaudhuri, R.G.; Paria, S. Synthesis of sulfur nanoparticles in aqueous surfactant solutions. *J. Colloid Interface Sci.* **2010**, *343*, 439–446. [[CrossRef](#)]
6. Li, W.; Zheng, G.; Yang, Y.; Seh, Z.W.; Liu, N.; Cui, Y. High-performance hollow sulfur nanostructured battery cathode through a scalable, room temperature, one-step, bottom-up approach. *Proc. Natl. Acad. Sci. USA* **2013**, *110*, 7148–7153. [[CrossRef](#)] [[PubMed](#)]
7. Suleiman, M.; Ali, A.A.; Hussein, A.; Hammouti, B.; Hadda, T.B.; Warad, I. Sulfur Nanoparticles: Synthesis, Characterizations and their Applications. *J. Mater. Environ. Sci.* **2013**, *4*, 1029–1033.
8. Cheng, X.; Cheng, K.; Liu, J.; Sun, X. Synthesis and characterizations of nanoparticle sulfur Using eggshell membrane as template. *Mater. Sci. Forum* **2011**, *675–677*, 279–282. [[CrossRef](#)]
9. Chaudhuri, R.G.; Paria, S. Growth kinetics of sulfur nanoparticles in aqueous surfactant solutions. *J. Colloid Interface Sci.* **2011**, *354*, 563–569. [[CrossRef](#)]
10. De Caprariis, B.; Di Rita, M.; Stoller, M.; Verdone, N.; Chianese, A. Reaction-precipitation by a spinning disc reactor: Influence of hydrodynamics on nanoparticles production. *Chem. Eng. Sci.* **2012**, *76*, 73–80. [[CrossRef](#)]
11. De Caprariis, B.; Stoller, M.; Chianese, A.; Verdone, N. CFD model of a spinning disk reactor for nanoparticle production. *Chem. Eng. Trans.* **2015**, *43*, 757–762.
12. Heng, G.; Yang, Y.; Cha, J.J.; Hong, S.S.; Cui, Y. Hollow carbon nanofiber-encapsulated sulfur cathodes for high specific capacity rechargeable lithium batteries. *Nano Lett.* **2011**, *11*, 4462–4467.
13. Guo, J.; Xu, Y.; Wang, C. Sulfur-impregnated disordered carbon nano-tubes cathode for lithium-sulfur batteries. *Nano Lett.* **2011**, *11*, 4288–4294. [[CrossRef](#)] [[PubMed](#)]
14. Liwen, J.; Rao, M.; Aloni, S.; Wang, L.; Cairns, E.J.; Zhang, Y. Porous carbon nanofiber-sulfur composite electrodes for lithium/sulfur cells. *Energy Environ. Sci.* **2011**, *4*, 5053–5059.
15. Elazari, R.; Salitra, G.; Garsuch, A.; Panchenko, A.; Aurbach, D. Sulfur-impregnated activated carbon fiber cloth as a binder-free cathode for rechargeable Li-S batteries. *Adv. Mater.* **2011**, *23*, 5641–5644. [[CrossRef](#)] [[PubMed](#)]
16. Demir-Cakan, R.; Morcrette, M.; Nouar, F.; Davoisne, C.; Devic, T.; Gonbeau, D.; Dominko, R.; Serre, C.; Férey, G.; Tarascon, J.M. Cathode composites for Li-S batteries via the use of oxygenated porous architectures. *J. Am. Chem. Soc.* **2011**, *133*, 16154–16160. [[CrossRef](#)]
17. Xiao, L.; Cao, Y.; Xiao, J.; Schwenzler, B.; Engelhard, M.H.; Saraf, L.V.; Nie, Z.; Exarhos, G.J.; Liu, J. A soft approach to encapsulate sulfur: Polyaniline nanotubes for lithium-sulfur batteries with long cycle life. *Adv. Mater.* **2012**, *24*, 1176–1181. [[CrossRef](#)] [[PubMed](#)]
18. Liwen, J.; Rao, M.; Zheng, H.; Zhang, L.; Dua, Y.L.W.; Guo, J.; Cairns, E.J.; Zhang, Y. Graphene oxide as a sulfur immobilizer in high performance lithium/sulfur cells. *J. Am. Chem. Soc.* **2011**, *133*, 18522–18525.

19. Wang, H.; Yang, Y.; Liang, Y.; Robinson, J.T.; Li, Y.; Jackson, A.; Cui, Y.; Dai, H. Graphene-wrapped sulfur particles as a rechargeable lithium-sulfur battery cathode material with high capacity and cycling stability. *Nano Lett.* **2011**, *11*, 2644–2647. [[CrossRef](#)]
20. Jayaprakash, N.; Shen, J.; Moganty, S.S.; Corona, A.; Archer, L.A. Porous hollow carbon-sulfur composites for high-power lithium-sulfur batteries. *Angew. Chem. Int. Ed.* **2011**, *50*, 5904–5908. [[CrossRef](#)]
21. Seh, Z.W.; Li, W.; Cha, J.J.; Zheng, G.; Yang, Y.; McDowell, M.T.; Hsu, P.C.; Cui, Y. Sulphur-TiO₂ yolk-shell nanoarchitecture with internal void space for long-cycle lithium-sulphur batteries. *Nat. Commun.* **2013**, *4*, 1331. [[CrossRef](#)]
22. Sun, T.; King, H.E. Aggregation behavior in the semidilute poly(N-vinyl-2-pyrrolidone)/water system. *Macromolecules* **1996**, *29*, 3175–3181. [[CrossRef](#)]
23. Qiu, P.; Mao, C. Biomimetic branched hollow fibers templated by self-assembled fibrous polyvinylpyrrolidone structures in aqueous solution. *ACS Nano* **2010**, *4*, 1573–1579. [[CrossRef](#)] [[PubMed](#)]
24. Xia, Y.; Wei, M.; Lu, Y. One-step fabrication of conductive poly(3,4-ethylenedioxythiophene) hollow spheres in the presence of poly(vinylpyrrolidone). *Synth. Met.* **2009**, *159*, 372–376. [[CrossRef](#)]
25. Aurbach, D.; Pollak, E.; Elazari, R.; Salitra, G.; Kelley, C.S.; Affinito, J. On the surface chemical aspects of very high energy density, rechargeable Li-sulfur batteries. *J. Electrochem. Soc.* **2009**, *156*, A694–A702. [[CrossRef](#)]
26. Dell’Era, A.; Pasquali, M.; Bauer, E.M.; Cipriotti Vecchio, S.; Scaramuzzo, F.A.; Lupi, C. Synthesis, characterization, and electrochemical behavior of LiMn_xFe_(1-x)PO₄ composites obtained from phenylphosphonate-based organic-inorganic hybrids. *Materials* **2018**, *11*, 56. [[CrossRef](#)] [[PubMed](#)]
27. Parola, V.; Liveri, V.T.; Todaro, L.; Lombardo, D.; Bauer, E.M.; Dell’Era, A.; Longo, A.; Caschera, D.; De Caro, T.; Toro, R.G.; et al. Iron and lithium-iron alkyl phosphates as nanostructured material for rechargeable batteries. *Mater. Lett.* **2018**, *220*, 58–61. [[CrossRef](#)]
28. Dell’Era, A.; Pasquali, M.; Tarquini, G.; Scaramuzzo, F.A.; De Gasperis, P.; Prosini, P.P.; Mezzi, A.; Tuffi, R.; Cafiero, L. Carbon powder material obtained from an innovative high pressure water jet recycling process of tires used as anode in alkali ion (Li, Na) batteries. *Solid State Ionics* **2018**, *324*, 20–27. [[CrossRef](#)]
29. Dell’Era, A.; Mura, F.; Pasquali, M.; Pozio, A.; Zaza, F. Synthesis and characterization of TiO₂ nanotubes as anodic material in lithium-ion batteries. *Nuovo Cimento Soc. Ital. Fis. C* **2013**, *36*, 65–72.
30. Pasquali, M.; Dell’Era, A.; Prosini, P.P. Fitting of the Voltage-Li⁺ insertion curve of LiFePO₄. *J. Solid State Electrochem.* **2009**, *13*, 1859–1865. [[CrossRef](#)]
31. Orecchini, F.; Santiangeli, A.; Dell’Era, A. EVs and HEVs Using Lithium-Ion Batteries. In *Lithium-Ion Batteries: Advances and Applications*; Pistoia, G., Ed.; Elsevier, B.V.: Amsterdam, The Netherlands, 2014; pp. 205–248.
32. Scaramuzzo, F.A.; Pasquali, M.; Mura, F.; Pozio, A.; Dell’Era, A.; Curulli, A. TiO₂ nanotubes photo-anode: An innovative cell design. *Chem. Eng. Trans.* **2014**, *41*, 223–228.
33. Scaramuzzo, F.A.; Pozio, A.; Masci, A.; Mura, F.; Dell’Era, A.; Curulli, A.; Pasquali, M. Efficient photocurrent generation using a combined Ni-TiO₂ nanotube anode. *J. Appl. Electrochem.* **2015**, *45*, 727–733. [[CrossRef](#)]
34. Scaramuzzo, F.A.; Dell’Era, A.; Tarquini, G.; Caminiti, R.; Ballirano, P.; Pasquali, M. Phase transition of TiO₂ nanotubes: A X-ray study as a function of temperature. *J. Phys. Chem. C* **2017**, *121*, 24871–24876. [[CrossRef](#)]
35. Santiangeli, A.; Fiori, C.; Zuccari, F.; Dell’Era, A.; Orecchini, F.; D’Orazio, A. Experimental analysis of the auxiliaries consumption in the Energy balance of a pre-series plug-in hybrid-electric vehicle. *Energy Procedia* **2014**, *45*, 779–788.
36. Pasquali, M.; Dell’Era, A.; Bauer, E.M.; Bellitto, C.; Righini, G.; Prosini, P.P. A versatile method of preparation of Carbon-rich LiFePO₄: A promising cathode material for Li-ion batteries. *J. Power Sources* **2005**, *146*, 544–549. [[CrossRef](#)]
37. Turganbay, S.; Aidarova, S.B.; Bekturganova, N.E.; Alimbekova, G.K.; Musabekov, K.B.; Kumargalieva, S.S. Surface-modification of sulfur nanoparticle with surfactants and application in agriculture. *Adv. Mater. Res.* **2013**, *785–786*, 475–479. [[CrossRef](#)]
38. Martynková, G.S.; Chrobáček, K.; Pazourková, L.; Aydina, S.; Pivoňka, D.; Novosad, B. Sulfur cathode material conductivity improving by carbon admixture: Technology and characterization. *Mater. Today Proc.* **2018**, *5*, S109–S114. [[CrossRef](#)]

39. Manthiram, A.; Fu, Y.; Chung, S.H.; Zu, C.; Su, Y.S. Rechargeable Lithium-Sulfur Batteries. *Chem. Rev.* **2014**, *114*, 11751–11787. [[CrossRef](#)] [[PubMed](#)]
40. Evers, S.; Yim, T.; Nazar, L.F. Understanding the nature of absorption/adsorption in nanoporous polysulfide sorbents for the Li-S battery. *J. Phys. Chem. C* **2012**, *116*, 19653–19658. [[CrossRef](#)]



© 2019 by the authors. Licensee MDPI, Basel, Switzerland. This article is an open access article distributed under the terms and conditions of the Creative Commons Attribution (CC BY) license (<http://creativecommons.org/licenses/by/4.0/>).